Organic Sol–Gel Process

DOI: 10.1002/anie.201002609

Organic Sol–Gel Synthesis: Solution-Processable Microporous Organic Networks**

*Su-Young Moon, Jae-Sung Bae, Eunkyung Jeon, and Ji-Woong Park**

Polymerization of rigid organic building blocks with multiple reactive functional groups yields microporous organic networks[1–6] whose pore sizes approach molecular length scales. Because molecules may be selectively adsorbed or transported inside these pores, the networks are promising for molecular storage, separation, delivery, or catalysis.

However, most of the organic networks synthesized to date were produced as intractable solids and therefore their post-processing and chemical functionalization were limited. Recent research on use of the networks concern mainly storage or capture of molecules in their as-produced solid forms.[7–12]

Here we present the first sol–gel-processable, microporous organic molecular networks which are synthesized by a two-stage mechanism involving the formation of colloidal dispersions and the subsequent growth to monolithic networks by solvent evaporation, analogous to the sol–gel synthesis of inorganic oxide networks. The resultant microporous organic networks, the pore functionality of which may be tunable by varying the constituent molecular units, are readily processable into coatings, free-standing films, nanoparticles with desired surface functionalities, and nanocomposites with other polymer matrices.

Microporous organic materials composed of rigid covalent networks include covalent organic frameworks (COF),[1,2,6–8,13] polymers of intrinsic microporosity (PIMs),[5,14–16] hyper-cross-linked polymers (HCPs),[12,17–19] and other polymer networks.[3,4,15,20,21] If these organic networks were made solution-processable without sacrificing their thermal or dimensional stability, their unique microporosity could be exploited for a broad range of applications. In particular, solution-processable covalent organic networks may provide novel molecular separation membranes, which were thought to be offered only by porous organics with non-network structures.[22,23]

For inorganic oxide networks, solution processing is enabled by the sol–gel mechanism,[24,25] in which the networks grow in a fractal manner by hydrolysis and condensation of monomers in the early stage of reaction, and then further monomer consumption leads to colloidal dispersions (sols) which, upon evaporation of the solvent, yield bulk networks by interparticle condensation. In this regard, we introduce the first organic system that yields molecular networks by a sol–gel polymerization mechanism.

Figure 1 illustrates the general scheme of the organic sol–gel processing method. We employed condensation of amine and isocyanate monomer pairs containing tetrakis(4-aminophenyl)methane[26] or tetrakis(4-isocyanatophenyl)methane[27] as network former. The resultant networks consist of tetrahedral arms that are linked three dimensionally via urea moieties, −NHCONH−. The urea-forming condensation reaction is advantageous because the reaction can be performed at ambient temperature without releasing byproduct molecules that may be trapped inside the network.

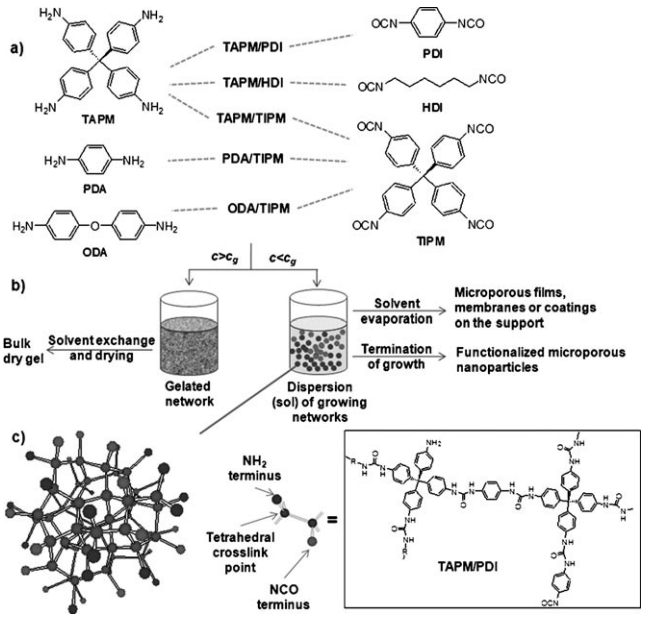

Figure 1. Sol–gel synthesis of organic molecular networks. a) Structures of the monomers and their combinations to yield 3D networks. b) Types of organic molecular networks produced by sol–gel versus direct gel-forming route. c) Model of a growing nanoparticle consisting of molecular network in the TAPM/PDI polymerization solution. In the model, gray, red, and blue circle designate the tetrahedral center, −NCO terminus, and $-NH_2$ terminus, respectively.

[*] S. Y. Moon, J. S. Bae, E. Jeon, Prof. J. W. Park
Department of Materials Science and Engineering
Gwangju Institute of Science and Technology
261 Cheomdan-gwagiro, Buk-gu, Gwangju, 500-712 (Korea)
Fax: (+82) 62-715-2314
E-mail: jiwoong@gist.ac.kr
Homepage: http://mse.gist.ac.kr/~snl/

[**] This research was supported by the Plant Technology Advancement Program (07seahero 02-03-01) funded by the Ministry of Land, Transport, and Maritime Affairs of the Korean government, and the Basic Science Research Program (2010-0000282) through the National Research Foundation of Korea (NRF) funded by the Ministry of Education, Science and Technology, and the Program for Integrated Molecular Systems (PIMS) at GIST.

Supporting information for this article is available on the WWW under http://dx.doi.org/10.1002/anie.201002609.

We hypothesized that the growing organic networks, if well-solvated by solvents, would not extend into the bulk solution below the critical gelation concentration c_g,[28] but rather would yield stable dispersions of microscopic particles. First we searched for gel-forming solvent systems for the five different amine/isocyanate monomer pairs that include at least one tetrahedral monomer (Figure 1a) by performing polymerization at high monomer concentration (> 0.1 g mL^{-1}). The solutions of all amine/isocyanate monomer pairs in the solvents such as DMF, dimethylacetamide, DMSO, or *N*-methylpyrollidone turned to transparent gels when they were mixed and stirred for a short time, whereas in other solvents such as THF, solid precipitates formed immediately on mixing the monomer solutions. The hydrogen-bonding capability of the solvents with urea groups must be crucial for stabilization of the growing networks against aggregation.

To establish the sol state of the organic networks, we ran many batches of polymerization for each monomer system with variation of its initial concentration. We obtained the gelation time t_g for each monomer combination for a range of initial monomer concentrations c (Figure 2a) by measuring the time elapsed until the gel was first visually observed at room temperature. The state of a reaction mixture was monitored until it became gel or for at least for one month under inert atmosphere if it did not gelate. Gelation was significantly delayed or even unobserved on lowering the initial monomer concentrations. Figure 2a shows that the critical gelation concentrations c_g, below which the mixture remained in the fluid phase without gelation, can be estimated for all of the monomer combinations. The TAPM/HDI pair shows the highest c_g value (ca. 0.03 g mL^{-1}) among the five monomer combinations. Noteworthily, even at concentrations higher than c_g, the reaction mixtures remained in the fluid phase for substantial periods of time; for example, the solution containing 0.05 g mL^{-1} TAPM/HDI in DMF remained in the fluid state for more than 24 h before the solution became a gel.

Although the reaction mixtures stay in the fluid state, the amine and isocyanate groups continue to react to generate new urea bonds. We monitored the progress of the condensation reaction in solutions of TAPM/HDI with concentrations of 0.02, 0.04, and 0.07 g mL^{-1} in [D$_7$]DMF using ^{1}H NMR spectroscopy. The signals of the phenylene protons of the TAPM moiety shift downfield as amino groups react with isocyanate groups to form urea bonds (Figure 2b). In Figure 2c, amine-to-urea conversions α, estimated by ^{1}H NMR integration, are plotted as a function of reaction time t. At 0.02 g mL^{-1}, which is below c_g, the conversion increased approximately in two stages: an initial stage in which α increases rapidly to about 70%, and a second stage in which α slowly increases to a plateau of about 80% even after stirring for a prolonged time. At 0.04 and 0.07 g mL^{-1}, which are higher than c_g, the NMR data could not be obtained beyond the gel point, where the conversion reached about 80%.

The fluid state of the reaction mixture was indeed an organic sol. Dynamic light scattering (DLS) of the reaction mixtures with a concentration of 0.02 g mL^{-1} indicated that nanoparticles grew as the amine–isocyanate condensation

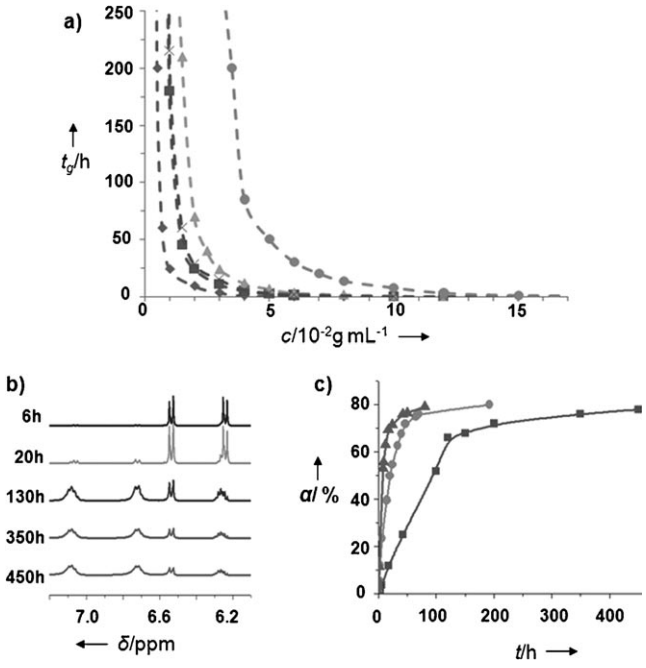

Figure 2. Progress of cross-linking polymerization in the organic sols. a) Gelation time t_g for solutions of five monomer pairs in DMF as a function of initial monomer concentration. Diamonds: TAPM/TIPM, squares: PDA/TIPM, triangles: TAPM/PDI, crosses: ODA/TIPM, and circles: TAPM/HDI. b) ^{1}H NMR spectra of the TAPM/HDI solution in [D$_7$]DMF recorded at reaction times of 6, 20, 130, 350, and 450 h. c) Conversion α as a function of reaction time t for TAPM/HDI solutions with different concentrations. Squares: 0.02, circles: 0.04, and triangles: 0.07 g mL^{-1}. The conversion was estimated by the percentage ^{1}H NMR spectrum integration for urea phenylene with respect to that of total phenylene groups.

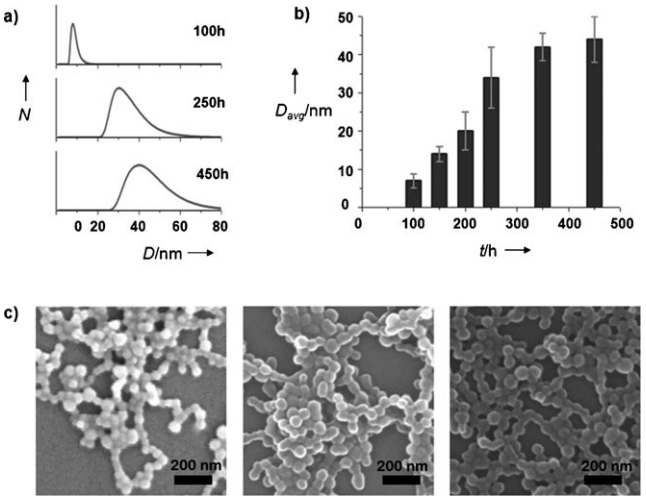

Figure 3. Growth of the nanoparticles composed of TAPM/HDI molecular networks in the sol state. a) Number distribution N of particle diameter D obtained from DLS measurements at reaction time t = 100, 250, and 450 h. b) Average DLS particle diameter D_{avg} as a function of reaction time t. c) SEM images of the nanoparticles of the network deactivated at t = 150, 250, and 450 h, from left to right, respectively.

reaction proceeded (Figure 3a). The particle size continued to grow even after the rate of the coupling reaction decreased significantly. By adding a small amount of water to the sol (see Experimental section), the residual isocyanate groups on the nanoparticles are converted to amino groups with loss of carbon dioxide. The particles stopped growing after this treatment and the DLS diameters of the deactivated particles remained nearly unchanged even for several months in solution. The size of the deactivated nanoparticles in the SEM images match reasonably well their DLS diameter measured immediately before deactivation (Figure 3c).

The apparent two-stage kinetics of amine–isocyanate coupling reaction and the rapid particle growth in the slow regime of the coupling reaction are accounted for by the presence of different reacting species contributing to the NMR-estimated conversion in the early and late stages. In the early stage the reaction occurs predominantly by consumption of the monomers or oligomeric networks that are sufficiently mobile and flexible to be capable of rapid intra- or intermolecular condensation reaction. Once most of these labile functional groups have been consumed, the reaction is governed by the coupling of residual functional groups, segmental motion of which is restricted by the network. This late-stage reaction includes interparticle coupling, whose rate depends on the concentration and the translational diffusivity of the particles and the rigidity of the constituent networks to which unconverted functional groups are pendent. It is therefore likely that smaller particles or those consisting of more flexible networks are preferably consumed to yield larger ones or those of more rigid networks. Interparticle coupling, even at a slow rate, results in significant increase of average particle size, which is indeed revealed by the DLS data shown in Figure 3a and b. Below c_g, the interparticle coupling rate must be negligibly small so that the mixture can remain in the sol state.

Thin coatings on solid substrates or free-standing films of the organic networks could be readily produced by depositing the organic sols and then evaporating the solvent. Because interparticle condensation resumes when the solvent is evaporated from the organic sols, the resulting films become monolithic networks that are insoluble in all solvents. The sols from all monomer pairs provided uniform coatings on flat substrates when the reaction conversion at the time of casting became higher than approximately 30%. The thickness of the resultant films ranged from a few hundred nanometers to a few hundred micrometers, and those thicker than several micrometers could be removed from the substrate to yield free-standing films. Figure 4 shows an optical photograph and SEM images of a free-standing film of TAPM/HDI network. The optical transparency of the films and the cross-sectional SEM image both indicate that the films have smooth morphology on the nanometer scale. The monomer pairs containing an aliphatic compound (HDI) gave more flexible free-standing films than other, rigid pairs. Even rigid monomer pairs such as TAPM/TIPM yielded uniformly smooth films on the substrate surface, although their free-standing films were relatively brittle compared with the TAPM/HDI network (Supporting Information, Figure S4). Porous substrates such as nonwoven fabrics or PTFE membranes could also be coated with the network films (Figures S5 and S6). The films exhibited high chemical and thermal stability: they showed nearly no dimensional change after treatments such as immersion in DMF for two days with stirring, or heating in an oven for 24 h at 200 °C. The thermal degradation temperature of all film samples appeared be near 300 °C according to thermogravimetric analysis (TGA, Figure 4c).

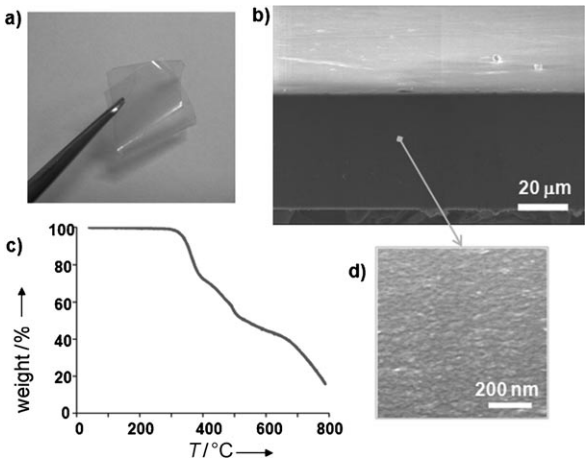

Figure 4. Free-standing film of the TAPM/HDI network. The film was obtained by evaporating a 0.04 g mL^{-1} sol mixture stirred for 24 h on a glass plate. a) Optical photograph of a rectangular film with an approximate size of 2×5 cm. b) SEM image of top and cross-sectional surface of fractured 48 μm-thick film supported on carbon tape. c) TGA curve of the film recorded under nitrogen with a heating rate of 10 °C min^{-1}. d) High-magnification SEM image of the cross section of (b).

Overall, the mechanism consisting of the formation of nanoparticle dispersions (sols) and subsequent condensation into monolithic networks by solvent evaporation is an exact replica of the sol–gel process[25] that was previously known only in inorganic systems.

The sol–gel-processed organic molecular networks exhibited microporosity, as was observed in other organic networks such as PIMs and COFs. Distinct from other network materials, we could prepare particulate samples by precipitation of the sols into a nonsolvent (acetone or methyl alcohol) followed by washing with the same solvent and drying under high vacuum at 200 °C. Thermal degradation temperatures of the particulate samples were also around 300 °C, similar to those of films (Figure S7). The particulate materials obtained from all monomer pairs gave carbon dioxide adsorption isotherms at 273 K indicative of microporosity (Figure 5a). Specific surface areas in the range of 200–600 m^{2}g^{-1} were estimated by applying the Dubinin–Astakhov (DA) equation to the adsorption isotherms (Table S1). The pore size and pore volume of the networks were typically in the range of 5–9 Å, and 0.1–0.3 cm^3 g^{-1}, respectively (Table S1 and Figure S3). We attribute our failure to obtain N_2 adsorption isotherms at 77 K to low diffusivity of nitrogen into the narrow pores, which are likely constricted by hydrogen bonding at cryogenic temperature.[16,29] Carbon dioxide is used preferably over nitrogen

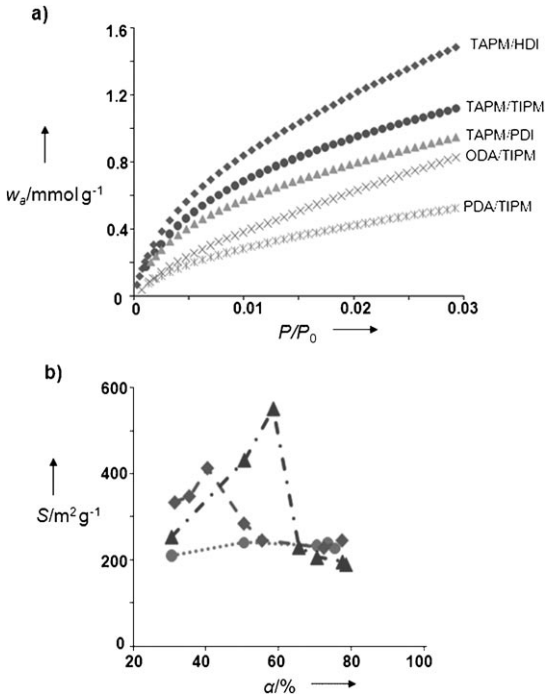

Figure 5. Microporous characteristics of organic molecular networks. a) Carbon dioxide adsorption isotherms measured at 273 K for various networks precipitated from their sol states; w_a is the quantity of carbon dioxide adsorbed. The preparation condition for each sample (monomer concentration, elapsed reaction time when deactivated) are (0.04 g mL^{-1}, 12 h) for TAPM/HDI, (0.005 g mL^{-1}, 10 h) for TAPM/TIPM, (0.02 g mL^{-1}, 24 h) for TAPM/PDI, (0.01 g mL^{-1}, 10 h) for ODA/TIPM, and (0.01 g mL^{-1}, 5 h) for PDA/TIPM.; b) Specific surface area S for the TAPM/HDI networks as a function of conversion α at the time of deactivation for three different initial monomer concentrations: circles 0.02, diamonds 0.04, and triangles 0.07 g mL^{-1}.

for these samples because of its facilitated adsorption onto polar sites within the polyurea network.[30]

Interestingly, the porosities of the particulate materials produced from their sols vary with the conversion of the network-forming reaction and exhibit maxima at intermediate conversions (Figure 5b). While clear understanding of these phenomena is yet to be sought, this result indicates that the network microporosity can be adjusted and optimized by altering the conditions employed for the sol–gel method.

We confirmed the presence of microporosity in film samples for two monomer pairs, TAPM/HDI and TAPM/TIPM, by means of their CO_2 adsorption curves (Figure S8). Not all of the film samples yielded reasonable adsorption curves. Several processing parameters of the films, which include the thicknesses of the films, the reaction conversion at the time of casting, and the conditions of activating the samples, may have to be further considered to obtain meaningful porosity data. In addition, it is uncertain that an identical technique should be used to measure the porosity of both the particulate and film samples. Nonetheless, the films obtained via the organic sol–gel route most likely consist of microporous networks similar to those of their corresponding nanoparticles in the sol state, and their ability to form coatings on various substrate surfaces is promising for fabrication of new solvent-resistant membranes for selective filtration on the molecular or nanoscopic level.[31]

Another important aspect of the current organic sol–gel method are the microporous nanoparticles themselves. The practical limit of conversion at about 80% indicates that about 20% of the starting aminophenyl groups and an equivalent amount of isocyanate groups remain intact in the sol state. These residual functional groups are likely located near the exterior of each nanoparticle, and are available for reaction with surface-modifying agents. For example, addition of an aliphatic acyl halide to the dispersion of nanoparticles gave alkyl-substituted nanoparticles of similar size that could be well dispersed in solvents (Supporting Information, Section G and Figures S9 and S10). These nanoparticles can be readily blended with other polymers to yield new nanocomposite materials. This dispersibility of the microporous nanoparticles in liquid or solid matrices is promising for their potential application as molecular-delivery or -separation media. Detailed studies on the functionalization of microporous particles are underway.

The findings of the present experiments on the organic sol–gel process suggest that various microporous organic networks can be obtained as colloidal dispersions provided that the growing networks can be well-solvated with solvent molecules. In addition to the facile processability of the molecular networks into nanoparticles, films, or membranes, our organic sol–gel method can be exploited further by combining it with conventional material-modification strategies such as chemical functionalization of the particle surface and blending or hybridization with other classes of functional materials.

Experimental Section

Sol–gel polymerization: In a typical run with TAPM/HDI at a concentration of 0.04 g mL^{-1}, tetrakis(4-aminopheyl)methane (TAPM) (0.1063 g,0.279 mmol) was dissolved in 2.5 mL of anhydrous DMF under a nitrogen atmosphere at room temperature. This solution was added, with stirring, to a solution of distilled hexamethylene diisocyanate (HDI, 0.0940 g, 0.558 mmol) in anhydrous DMF (2.5 mL) at room temperature. The reaction mixtures remained in the fluid state (sol) up to the gelation time t_g, which in this case was about 85 h. The nanoparticle aggregates were obtained by precipitation of the sol at a designated reaction time into a nonsolvent (acetone). The precipitate was stirred in pure acetone and collected by filtration (repeated 4 times). The resulting powders were then dried under high vacuum at 50 °C for 1 h, 100 °C for 1 h, and 200 °C for 48 h. To obtain bulk dry gel samples, the wet gel (formed after 85 h) was poured into acetone followed by the same purification procedure as the sample from the sol state. Free-standing films and coatings on substrates were prepared by casting from the sol state and subsequent solvent evaporation at 80 °C under nitrogen flow.

Received: April 30, 2010
Revised: June 9, 2010
Published online: August 30, 2010

Keywords: microporous materials · nanoparticles · polycondensation · sol–gel processes · thin films

[1] H. M. El-Kaderi, J. R. Hunt, J. L. Mendoza-Cortes, A. P. Cote, R. E. Taylor, M. O'Keeffe, O. M. Yaghi, *Science* **2007**, *316*, 268.
[2] A. P. Cote, A. I. Benin, N. W. Ockwig, M. O'Keeffe, A. J. Matzger, O. M. Yaghi, *Science* **2005**, *310*, 1166.
[3] J. X. Jiang, F. Su, A. Trewin, C. D. Wood, H. Niu, J. T. A. Jones, Y. Z. Khimyak, A. I. Cooper, *J. Am. Chem. Soc.* **2008**, *130*, 7710.
[4] E. Stöckel, X. F. Wu, A. Trewin, C. D. Wood, R. Clowes, N. L. Campbell, J. T. A. Jones, Y. Z. Khimyak, D. J. Adams, A. I. Cooper, *Chem. Commun.* **2009**, 212.
[5] N. B. McKeown, B. Gahnem, K. J. Msayib, P. M. Budd, C. E. Tattershall, K. Mahmood, S. Tan, D. Book, H. W. Langmi, A. Walton, *Angew. Chem.* **2006**, *118*, 1836; *Angew. Chem. Int. Ed.* **2006**, *45*, 1804.
[6] R. W. Tilford, S. J. Mugavero, P. J. Pellechia, J. J. Lavigne, *Adv. Mater.* **2008**, *20*, 2741.
[7] H. Furukawa, O. M. Yaghi, *J. Am. Chem. Soc.* **2009**, *131*, 8875.
[8] S. S. Han, H. Furukawa, O. M. Yaghi, W. A. Goddard, *J. Am. Chem. Soc.* **2008**, *130*, 11580.
[9] A. Thomas, P. Kuhn, J. Weber, M. M. Titirici, M. Antonietti, *Macromol. Rapid Commun.* **2009**, *30*, 221.
[10] J. Germain, J. M. J. Frechet, F. Svec, *Small* **2009**, *5*, 1098.
[11] A. W. C. van den Berg, C. O. Arean, *Chem. Commun.* **2008**, 668.
[12] C. D. Wood, B. Tan, A. Trewin, F. Su, M. J. Rosseinsky, D. Bradshaw, Y. Sun, L. Zhou, A. I. Cooper, *Adv. Mater.* **2008**, *20*, 1916.
[13] S. Wan, J. Guo, J. Kim, H. Ihee, D. L. Jiang, *Angew. Chem.* **2008**, *120*, 8958; *Angew. Chem. Int. Ed.* **2008**, *47*, 8826.
[14] M. G. Schwab, B. Fassbender, H. W. Spiess, A. Thomas, X. L. Feng, K. Mullen, *J. Am. Chem. Soc.* **2009**, *131*, 7216.
[15] P. Kuhn, M. Antonietti, A. Thomas, *Angew. Chem.* **2008**, *120*, 3499; *Angew. Chem. Int. Ed.* **2008**, *47*, 3450.
[16] J. Weber, M. Antonietti, A. Thomas, *Macromolecules* **2008**, *41*, 2880.
[17] J. H. Ahn, J. E. Jang, C. G. Oh, S. K. Ihm, J. Cortez, D. C. Sherrington, *Macromolecules* **2006**, *39*, 627.
[18] J. Germain, J. Hradil, J. M. J. Frechet, F. Svec, *Chem. Mater.* **2006**, *18*, 4430.
[19] J. Y. Lee, C. D. Wood, D. Bradshaw, M. J. Rosseinsky, A. I. Cooper, *Chem. Commun.* **2006**, 2670.
[20] A. I. Cooper, *Adv. Mater.* **2009**, *21*, 1291.
[21] J. Schmidt, J. Weber, J. D. Epping, M. Antonietti, A. Thomas, *Adv. Mater.* **2009**, *21*, 702.
[22] P. M. Budd, B. S. Ghanem, S. Makhseed, N. B. McKeown, K. J. Msayib, C. E. Tattershall, *Chem. Commun.* **2004**, 230.
[23] T. Tozawa, J. T. A. Jones, S. I. Swamy, S. Jiang, D. J. Adams, S. Shakespeare, R. Clowes, D. Bradshaw, T. Hasell, S. Y. Chong, C. Tang, S. Thompson, J. Parker, A. Trewin, J. Bacsa, A. M. Z. Slawin, A. Steiner, A. I. Cooper, *Nat. Mater.* **2009**, *8*, 973.
[24] C. J. Brinker, K. D. Keefer, D. W. Schaefer, R. A. Assink, B. D. Kay, C. S. Ashley, *J. Non-Cryst. Solids* **1984**, *63*, 45.
[25] L. L. Hench, J. K. West, *Chem. Rev.* **1990**, *90*, 33.
[26] P. Ganesan, X. N. Yang, J. Loos, T. J. Savenije, R. D. Abellon, H. Zuilhof, E. J. R. Sudholter, *J. Am. Chem. Soc.* **2005**, *127*, 14530.
[27] D. Laliberté, T. Maris, J. D. Wuest, *Can. J. Chem.* **2004**, *82*, 386.
[28] P. J. Lu, E. Zaccarelli, F. Ciulla, A. B. Schofield, F. Sciortino, D. A. Weitz, *Nature* **2008**, *453*, 499.
[29] D. Cazorla-Amorós, J. Alcaniz-Monge, A. Linares-Solano, *Langmuir* **1996**, *12*, 2820.
[30] J. F. Janik, W. C. Ackerman, R. T. Paine, D.-W. Hua, A. Maskara, D. M. Smith, *Langmuir* **1994**, *10*, 514.
[31] P. Vandezande, L. E. M. Gevers, I. F. J. Vankelecom, *Chem. Soc. Rev.* **2008**, *37*, 365.

